ISSN 2303-4521
Periodicals of Engineering and Natural Sciences *Original Research*
Vol. 12, No. 3, December 2024, pp.577-594

Automated detection of gait events using inertial sensor signals and a discrete wavelet transform approach

Humberto J. Navarro[1, 2], Wilson J. Arenas[2], Wilwer J. Jaimes[2], Sergio A. Salinas[2]
[1] Faculty of Natural Sciences and Engineering, Unidades Tecnológicas de Santander, Bucaramanga, Colombia
[2] Faculty of Electrical and Electronics Engineering, Universidad Pontificia Bolivariana, Bucaramanga, Colombia

ABSTRACT

Detection of gait cycle events is a crucial step toward an effective evaluation and rehabilitation of pathologies or injuries in human locomotion. Recently, methods based on the Discrete Wavelet Transform (DWT) have been useful for this detection due to their robustness and the wide variety of options for analyzing and decomposing signals in time/frequency domains, as well as their ability to extract relevant features embedded in the signals. In this study, a detection method of main gait cycle events, using the Wavelet Symlets and Daubechies families, was developed. These events are the heel-strike (HS) and the toe–off (TO). Inertial signals were acquired by three different devices: a G–WALK (reference equipment), an Apple Watch (AW), and a noncommercial device based on Inertial Measurement Units (IMUs). The dataset was obtained from six–minute walking tests performed by 22 healthy subjects. First, the dataset was processed, and then the signals were synchronized regarding the reference system. Subsequently, the signals were decomposed into 6 levels using sym4 and db5 Wavelets to obtain multiple perspectives of the signals. Then, using automatic threshold techniques and symmetric windows, it was possible to detect HS and TO events. Finally, the IMUs–based system obtained a 94.398 % of recall, 100 % of precision, and 97.117 % of $F_1-\text{score}$, with absolute values delays in the detection between 10–20 ms. In contrast, the AW system performance was 90.168 %, 100 %, and 94.828 % for recall, precision, and $F_1-\text{score}$, respectively, with absolute values delays in the detection of 10–28 ms.

Keywords: Apple Watch, Discrete Wavelet Transform, Gait Cycle, Inertial Sensors

Corresponding Author:

Humberto José Navarro Nigrinis
Unidades Tecnológicas de Santander
Calle de los Estudiantes #9-82, Bucaramanga
E-mail: hnavarro@correo.uts.edu.co

1. Introduction

Gait involves a sequence of movements that require a balance between neural and musculoskeletal systems [1]. The ability to walk is usually developed after the first year of human life. It is an action that involves almost all the muscles of the human body, as well as different cortical and subcortical brain structures, which helps to explain the extensive learning phase during childhood and the difficulty, or almost impossibility, of relearning after an injury. The importance of the analysis in the clinical area lies in the fact that human gait disorders account for approximately 55 % of all disabilities worldwide [2].

In the past few years, technological advances have made it possible to study abnormalities related to gait deficits associated with the aging of the population [3], motor disabilities in patients with cerebrovascular disease [4], [5], [6], [7], [8], [9], [10], and Parkinson's disease [11], [12], [13], [14]. In this context, gait systems built with inertial sensors are increasing their popularity in human gait analysis because 1) they allow quantitative measurement of locomotion systems [15], [16], 2) they allow assessment of the effect of a cognitive [17], [18] or biomechanical efforts [19], [20], [21], and 3) they are portable and low cost [6], [22], [23], [24]. In addition,

these devices can be used for longer analysis time periods in larger workspaces and increase comfort during the setup procedure [25], [26], [27], in comparison to controlled experimental environments, which use cramped spaces, resulting in higher equipment investment and can generate an unnatural gait.

We propose a method to detect the main events of human gait: heel-strike (HS) and toe–off (TO). This detection is based on processing angular velocity signals and a Discrete Wavelet Transform (DWT) approach. Independent signals were recorded by three different devices: two commercial devices, a G-WALK and an Apple Watch, and a non–commercial device based on inertial measurement units (IMU). The IMU–based gait measurement system was developed at the BISEMIC laboratory at Universidad Pontificia Bolivariana, Colombia. The accuracy of this non–commercial device was tested by Vargas [28], who obtained an average error of less than 15 % to measure five spatiotemporal parameters. On the other hand, the G–WALK was considered the reference device because it is specifically designed for gait analysis. Data acquisition was performed in a natural environment, where the subject was moving without speed restrictions, without markers attached, and wearing the three devices in different parts of their body. We used the processing of the signals coming from the inertial sensors and the synchronization of the dataset concerning the reference system presented in [29]. Then, we utilized families of Symlets and Daubechies Discrete Wavelet Transforms (DWT) to decompose the angular velocity signal into different frequency ranges. These levels of decomposition made it possible to visualize the signals in greater detail and under diverse perspectives, which led to a focus on extracting relevant features at the inflection points where the gait events of interest occur. Subsequently, automatic thresholding and symmetrical windowing techniques were applied to detect HS and TO events. Finally, through performance metrics, the algorithm developed was contrasted with the reference system.

2. Gait Analysis

To understand specific asymmetries related to the way we move and to determine pathologies or injuries in human locomotion, physicians and researchers often use gait analysis to evaluate and treat people with various conditions, pathologies, or injuries [30], [31], [32]. A standard gait evaluation requires at least one complete gait cycle, from when the heel makes contact with the ground to when it ends with the next contact of the heel of the same foot with the ground. Naturally, the more heel contacts analyzed, the better it will fit a constant set of natural heel contacts due to their inherent variability.

2.1. Human Gait Cycle

A complete analysis of human gait requires an understanding of the complete gait cycle, as illustrated in Figure 1, which is composed of two phases. The support phase or stance contains five phases: heel–strike (HS), foot–flat (FF), mid–stance (MSt), heel–off (HO), and toe–off (TO), which is the transition phase between the stance phase and the swing phase. The swing phase comprises three phases: initial swing, mid–swing (MSw), and terminal swing. The full human gait cycle has an average velocity in healthy adults of 1.20 m/s to 1.40 m/s. These variations will depend on a person's stride length and stride time [33], [34], [35]. The description of the cycle and the phases of the human march vary from one author to another. In the study, it was used the nomenclature defined in [36].

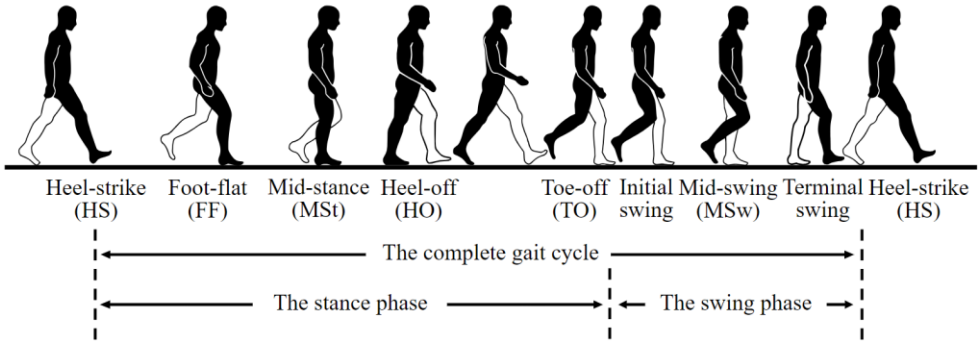

Figure 1. Human gait cycle and its lower limb events, based on [37].

2.2. Arm swing during the human gait cycle

The movement of the upper limbs is a typical characteristic of human gait. This balancing facilitates changes in gait speed and reduces the energy consumption of the muscles of the lower limbs [38]. During a normal gait cycle, the shoulder moves in a range of 20° to 30°, of which, 70 % or 80 % is in the direction of extension, and

the remaining 20 % or 30 % in flexion [36]. Figure 2 illustrates the gait cycle as seen from the arm swing and depicts the extension and flexion movements, the ipsilateral leg events, and the heel–strike of the contralateral leg (arrowhead).

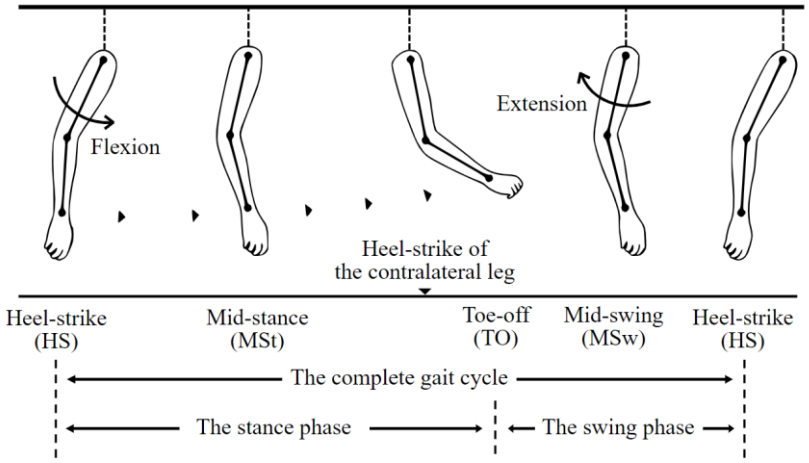

Figure 2. Relation between arm–swing positions and lower limb events, based on [39].

The arm swing parameters are illustrated in Figure 3, where the anteroposterior amplitude of the arm swing arc is measured from the coordinates of the wrist in the sagittal plane [39]. This amplitude consists of two movements: anterior and posterior, measured from the reference line (demarcated with the letter V) and labeled with positive and negative values (maximum and minimum), respectively. Furthermore, the phases of stance and swing (black and white bar, respectively) of the ipsilateral leg and the heel–strike of the contralateral leg (arrowhead). For the gait cycle events seen from the arm swing, the following is presented: the HS event of the right leg is characterized because the wrist has a negative decreasing angle in the extension direction and the TO event of the same leg occurs moments after reaching the maximum flexion of the wrist (HS event of the contralateral leg).

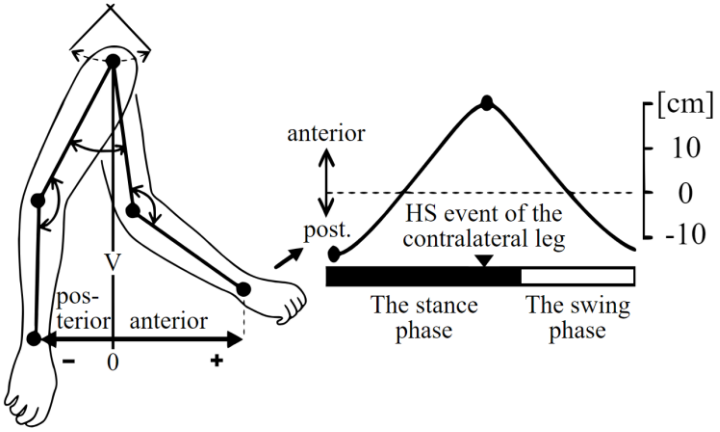

Figure 3. Amplitude of arm–swing during the gait cycle, based on [39].

2.3. Morphology of the angular velocity signal in the *z*–axis

For this study, the angular velocity signal of the mediolateral leg axis (*z*–axis) was considered when measurements were made with the IMU system located at the ankles since the morphology of the signal allows easier identification and detection of stance and swing phases and events of the human gait cycle [40], [41], [42]. Figure 4 (a) shows that the beginning of the stance phase is associated with the first heel–floor contact (marked in red). While the swing phase is associated with the contact of the toes with the floor, before the foot lift–off (marked in green). It is emphasized that these positions correspond to instantaneous equilibrium states, where the acceleration becomes zero, as evidenced by the tangent line in the respective HS and TO. In the case of the Apple Watch, no literature was found on the signal morphology, but based on the results reported in [38], [39], and because of the similarity it shares with the IMU signal in the *z*–axis, similar characteristics were identified. During the swing phase, a rebound was observed between the HS and TO events, due to the movement of the wrist in the flexion direction, similar to the rebound generated by the foot using the IMU system. While for the TO event, there was a negative angular velocity peak after the rebound. For the stance phase, it was found that the HS event presents a positive increasing angle because the wrist at that particular

instant of time reaches the maximum flexion, different from the IMU system, that occurs at a peak of negative angular velocity. Likewise, the gap between the movement of the leg and the wrist was detected. Figure 4 (b) illustrates the angular velocity signal for AW. For the G–WALK, being a specialized device for the study of human gait, the morphology was not described. The internal algorithms of this commercial system are part of the privacy of the company that produces it.

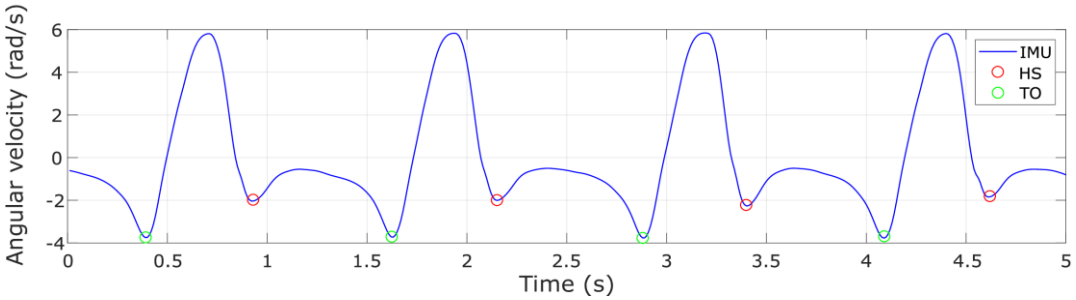

(a) Angular velocity signal on the *z*–axis of the IMU–L.

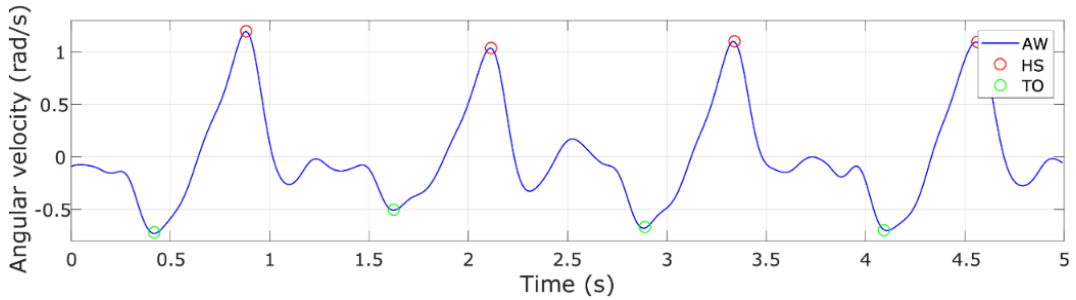

(b) Angular velocity signal on the *z*–axis of the AW–R.

Figure 4. Angular velocity signals on the *z*–axis with the gait events (HS and TO).

3. Materials and Methods

This section presents the materials and methods used to data acquisition and processing, automated detection of events, automatic thresholds and labeling HS and TO events.

3.1. Data acquisition and processing

The dataset was obtained from trials involving 22 healthy volunteers (16 men and 8 women), between the ages of 18 and 25 years. Each subject naturally walked overground over a 30–meter straight hallway at normal speed for 6 minutes, the trials were done twice time with 10–minute breaks. G–WALK sensor was placed on the spine (L5), AW smartwatches on each wrist, and IMU sensors were placed on each ankle, as shown in Figure 5.

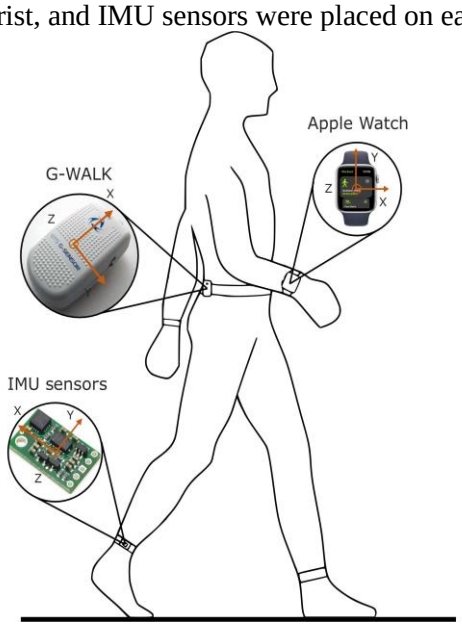

Figure 5. Location of the sensors in the subject.

The signals were obtained in an uncontrolled environment within the student community of the university, with prior authorization from the participants, and accepted by the ethics committee of the Universidad Pontificia Bolivariana–Campus Bucaramanga, Colombia. Figure 6 shows examples of these signals (accelerometer A and gyroscope G) for each axis (*x*, *y*, and *z*), G–WALK (marked in blue), AW (marked in red), and IMU (marked in green). These signals were acquired in different parts of the body, resulting in natural changes in the morphology of the signals. Each record of the dataset consists of six signals; corresponding to three acceleration and three gyroscope axes. The signals collected by the IMUs were obtained only for the three axes of the gyroscope. The beginning of the recording of the signals was different for the three systems. Therefore, the AW smartwatches and IMUs signals were not synchronized with the reference equipment. For this reason, the cross–correlation between the *z*–axis of the G–WALK and each angular velocity signal of the IMU–L and AW–R on the *z*–axis was used to estimate the delay and have all the signals aligned. In the case of large outliers generated by the motion of the turns, the function findpeaks was used to remove these outliers from the dataset. To extract the HS and TO events from the G–WALK angular velocity signals, the SMARTanalyzer® software was used. This software made it possible to load the signal and automatically obtain the moments in time in seconds where each event occurred. This process was performed for the 44 signals in the dataset. The procedure for signal processing and synchronization stages are detailed in [29].

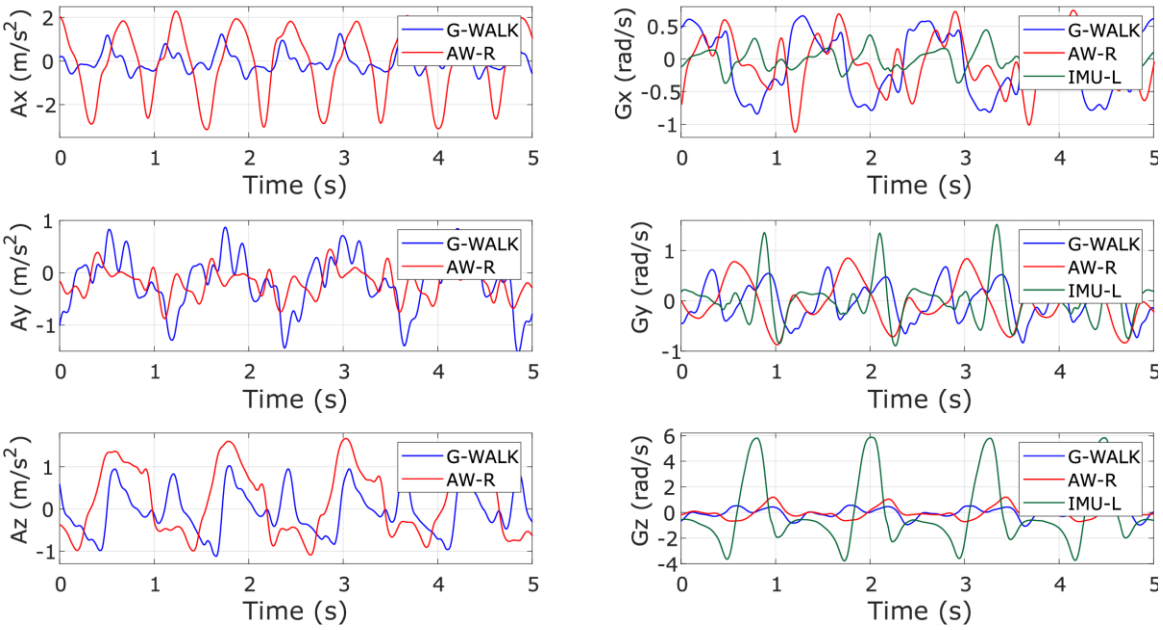

Figure 6. Inertial sensor signals (accelerometers on the left and gyroscopes on the right).

3.2. Automated detection of events of the human gait cycle

Once the synchronized and labeled dataset was obtained, it was necessary to develop a method of detection labeled, it was necessary to develop a DWT–based gait cycle event detection method, intending to compare it with the G–WALK reference system. To perform this task, two Wavelet families (Daubechies and Symlets) were used to detect human gait events [43], [44], [45], [46], [47]. Then, DWT was performed using the MATLAB® R2019a modwt function. The experiment setup parameters for the two families were as follows: for the Daubechies and Symlets mother Wavelets, the Wavelets db5 and sym4 were selected, correspondingly; both with 6 levels of decomposition, to extract the detail coefficients from d_4 to d_6 for AW and the IMU–based system. The first selection of the two families of mother Wavelets was made taking into account the similarity in the morphology with the angular velocity gait signal in the *z*–axis. The second selection was made considering the frequency ranges described in [29]. Additionally, the main characteristics of the gait signal were identified as the swing phase, which is characterized by a positive angular velocity and reaches its maximum value in the medium swing phase (MSw event). This maximum peak contributes to the improvement of event detection through windowing techniques for the IMU–based system. For the AW this peak was defined as an HS event, based on what is described in subsection 2.3. A negative angular velocity peak before reaching its maximum value (TO event), is associated with the last ground contact before the swing phase, and a negative angular velocity peak after reaching its maximum value (HS event, for the IMU–based system), occurs when the heel touches the ground [40], [41], [42]. The objective was based on preserving the aforementioned characteristics

and the frequency bands (B_f) described in Table 1, and eliminating the others, after applying DWT. The values described in Table 1 were constructed using Equation (1).

$$B_f = \frac{F_s}{2^n} \quad (1)$$

where F_s corresponds to the sampling frequency of the system and n corresponds to the decomposition levels.

Table 1. Frequency bands for each wavelet decomposition level.

Level	From (Hz)	To (Hz)	Coefficients
1	25.00	50.00	d_1
2	12.50	25.00	d_2
3	6.250	12.50	d_3
4	3.125	6.250	d_4
5	1.562	3.125	d_5
6	0.781	1.562	d_6

For the sub–bands coding phase, the transform is repeated several times to reduce the approximation coefficient of the sample in sub–bands, increasing frequency resolution. Each of the sub–bands of the signal contains information about different frequencies; such as abrupt changes in the higher frequency bands and minimal changes in the lower frequency bands. This allows us to obtain a transform between a frequency range of 0.781 Hz up to 6.250 Hz for AW and the IMU–based system. To extract the HS and TO events from the transformed signal, the imodwt function of MATLAB® R2019a was used to obtain the inverse DWT from the detail coefficients d_4 to d_6 and, finally, to obtain a reconstructed signal for the two acquisition systems between the mentioned frequency ranges.

3.3. Automatic thresholds

Once the reconstructed signals for AW and the IMU–based system were obtained, it was necessary to define automatic thresholds for the detection of the time instants where each event occurred. To perform this task, it was necessary to obtain the absolute square for each reconstructed signal, and from this, the median value and the standard deviation were determined. The automatic threshold was defined as the sum of these two values. To determine these thresholds were necessary to calculate the values within the interquartile range of each signal before obtaining the standard deviation and with this to make them more robust to the large outliers, and these thresholds could be adapted to the statistical characteristics of each of the signals. To facilitate the extraction of the HS and TO events, the MATLAB® R2019a findpeaks function was used to locate the positions of the MSw and HS events for the system based on IMUs and AW, respectively, taking into account the following configuration parameters: the minimum peak height was defined by the automatic threshold and the minimum distance between peaks was set to 1 s (100 samples). This selection was made taking into account that the angular velocity gait signal in the *z*–axis reaches its maximum value (MSw and HS event) approximately every 1.2 s, given that healthy patients usually walk at an average speed between 1.20 m/s to 1.40 m/s (full human gait cycle) [33], [34], [35]. The identification of the MSw peak contributed to minimizing the error in the detection of the HS and TO events for the IMU–based system. Likewise, detection of the HS event was achieved for the AW system, regardless of the sensor location, since these devices are located in different parts of the body, which causes changes in the morphology of the angular velocity signals.

After the MSw and HS peaks were identified, a symmetrical window of 40 samples was defined from the position obtained for both systems. The findpeaks function was then used to locate peaks only within the defined window range and a minimum peak–to–peak distance of 15 samples was set in order to extract HS and TO events for the IMU–based system, and TO for the AW, independently in an $n \times m$ matrix, where n corresponds to the number of rows and m to the number of columns. This selection was performed taking into account that approximately every 0.3 s an event of the human gait cycle occurs in healthy patients [33], [34]. This process was performed for the 44 signals obtained after DWT.

3.4. Labeling of other measurement systems based on DWT

Once the HS and TO event positions were obtained (new labels) for the 44 signals in the database using the DWT, it was necessary to generate a second set of labels based on the *z*–axis angular velocity signals for AW and the IMU–based system, to compare the generated labels with those of the reference system.

4. Results Evaluation Methodology

This section presents the methodology used to evaluate the performance of the proposed algorithm for the automated detection of HS and TO events.

4.1. Tolerance ranges in the detection of events

Tolerance ranges up to 50 ms have been described in the literature [15], [22], [48], [49]. To compare the estimates in the detection of gait events with the reference values, a symmetrical window of 30 ms was defined from each position of the events obtained by the standard equipment. If the event value found by the other systems was within the 30 ms range, it was considered a true positive (TP), otherwise, it was defined as a false positive (FP). This process was performed for the entire dataset.

4.2. Algorithm evaluation parameters

To evaluate the detection method, it was used a fundamental tool that allows visualization of the performance of a classification algorithm. This tool is the confusion matrix, which provides information on the number of hits and misses in detection, and shows whether the method is confused between events. Based on the information extracted from the confusion matrix, metrics such as recall, precision, and $\mathrm{F}_1-\mathrm{score}$ were obtained, which are fundamental to evaluating the performance of DWT–based detections [15], [23], [46], [50], [51], and, being a classification problem with significantly unbalanced classes, are suitable for not biased analysis to the majority class. Additionally, the time differences between the reference value and the other systems were calculated for each event, in order to obtain the average delay in detection for each event.

5. Results

5.1. Automated detection of human gait cycle events

After verification of the synchronization method, DWT was applied to each signal in the dataset using the Daubechies and Symlets Wavelet Families (db5 and sym4, respectively) with 6 levels of decomposition. This was done to extract only the detail coefficients from d_4 to d_6, which correspond to the frequency range of 0.781 Hz to 6.250 Hz. From this, the signal was reconstructed using the inverse DWT. DWT allowed the extraction of relevant features in the angular velocity signal in the *z*–axis, such as the maximum and minimum peaks where the time events of the gait cycle occur for the IMU–based system, as illustrated in Figure 7. For the AW system, two inflection points were found where the HS and TO events occur, based on the behavior of the signal and as described in [38], [39], as illustrated in Figure 8. From the figures, it can be observed that independent of the Wavelet Families used, the observed result is the same because Symlet Wavelets are a variant of Daubechies Wavelets [52], [53]. In addition, it can be observed that the relevant characteristics, such as maximum and minimum peaks of the transformed AW signals, are not completely defined compared to those of the IMU–based system, because, when performing the displacement of each wrist, the signals could be affected by factors such as stiffness and asymmetry in the upper limbs [45].

After applying DWT to the entire dataset, and obtaining the automatic threshold, it was possible to characterize the MSw and HS event for the system based on IMUs and AW, respectively, and obtain the maximum peaks, as illustrated in Figures 7 and 8 for IMU–L and AW–R respectively. The characterization of these two running events allowed us to optimize the localization of the other events (HS and TO) immersed in the signal within the defined interval. Once the positions of the maximum peaks of the transformed signal were obtained, a symmetrical window of 0.4 s was defined from the location of the peaks found, to find the equilibrium point between true positives and false positives, because if it is made smaller, true positives are minimized and if it is larger, false positives are maximized, and the findpeaks function was used, with a minimum peak–to–peak distance of 0.15 s. This allowed the detection of the two central events (HS and TO) for the IMU–based system and TO event for the AW. As a result of applying the windowing technique, the error in detection between events was minimized, due to the changes in magnitude caused by the location of the devices in different parts

of the body and the anatomical differences of each patient [30], [31], [54]. Figures 7 and 8 show the results of event detection using windowing techniques for the two acquisition systems (IMU–L and AW–R respectively).

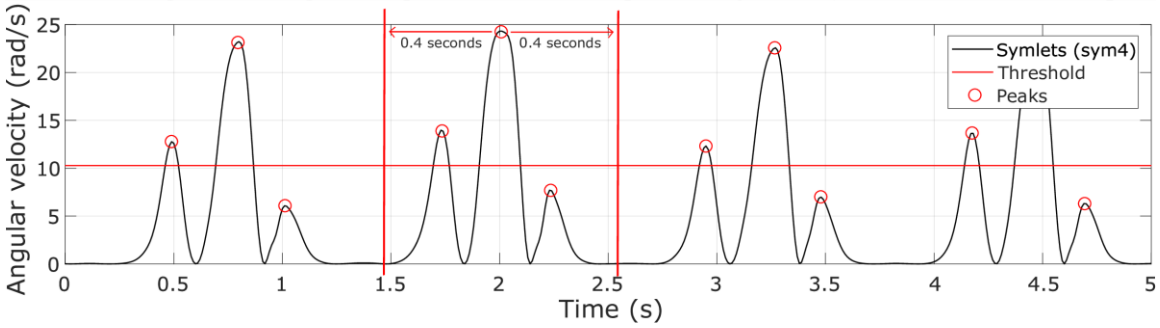

(a) Transformation of the IMU–L gyroscope signals with the automatic threshold and events detection using windowing (Symlets, sym4).

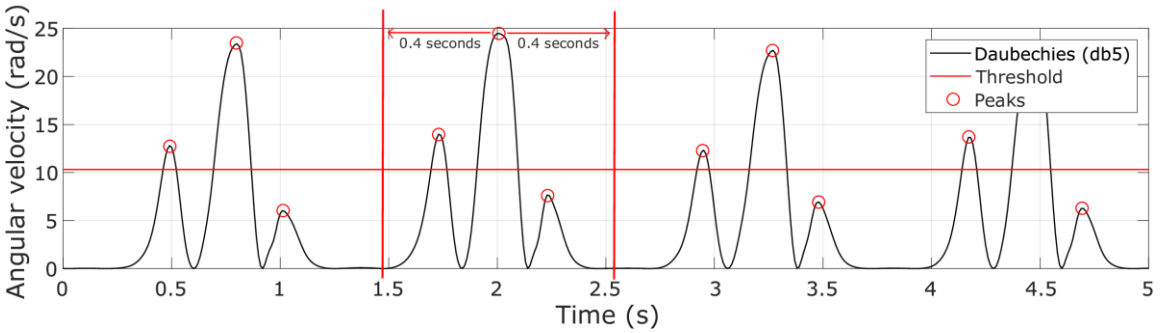

(b) Transformation of the IMU–L gyroscope signals with the automatic threshold and events detection using windowing (Daubechies, db5).

Figure 7. Automatic threshold, peak, and events detection using windowing in the IMU–L gyroscope transformations.

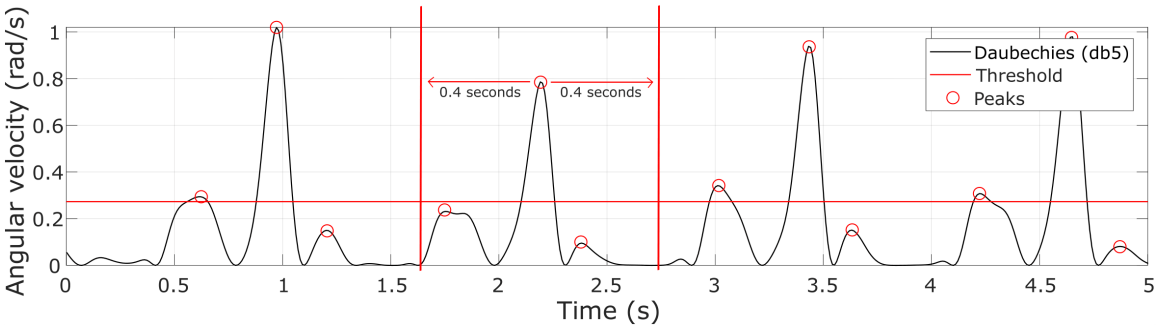

(a) Transformation of the AW–R gyroscope signals with the automatic threshold and events detection using windowing (Symlets, sym4).

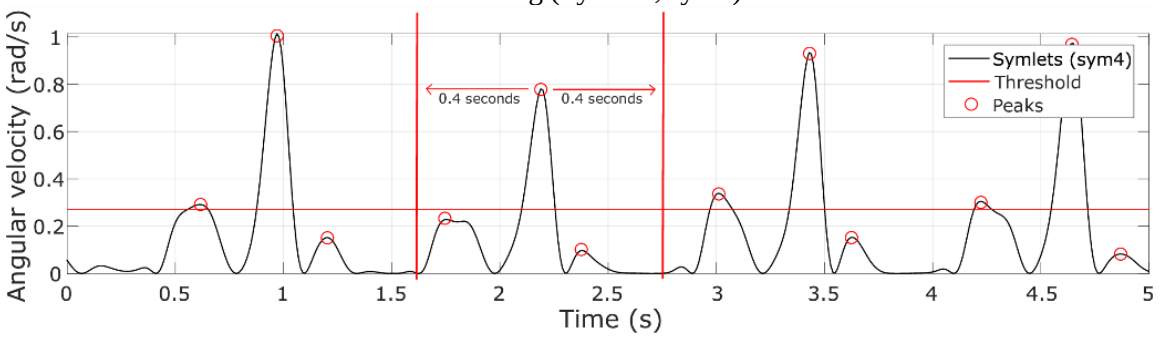

(b) Transformation of the AW–R gyroscope signals with the automatic threshold and events detection using windowing (Daubechies, db5).

Figure 8. Automatic threshold, peak, and events detection using windowing in the AW–R gyroscope transformations.

For the AW system, peaks of magnitude less than 0.16 rad/s were discarded, since these peaks do not correspond to central events of the gait cycle. From the figures, it can be seen that for the IMU–based system, the events were localized without any difficulty, because the inflection points are fully defined. that the inflection points are completely defined. For the AW system, the opposite happens, the maximum and minimum peaks are not defined and sometimes the TO event can have the same magnitude as other inflection points immersed in the signal, especially for AW–R signals. These abnormalities present in arm swing amplitude are related to factors such as walking speed, the relationship between arm swing kinematics, and asymmetric leg movements or by alterations that correlate with the presence or absence of disease [55]. Also, it is often assumed that arm swing is symmetrical in healthy people. Moreover, based on qualitative observations in [56] it was stated that the dominant hand moves less than the non-dominant hand during human gait.

With the detection of the events, the extracted positions were used to label the gait cycle events in the *z*–axis angular velocity signals for the IMUs and AW–based system as illustrated in Figure 9 (a) and Figure (b), respectively. From the figures, it can be seen that there is in fact a lag between the movement of the leg and the wrist, as was proposed at the beginning of the study. This difference is performed involuntarily by the human body because by oppositely moving the arms, the angular momentum of the body around the vertical axis is minimized and the turning movement produced by the body when moving forward is counteracted, likewise, it also softens the human gait and reduces the energy expenditure of the muscles of the lower extremities [57], [58].

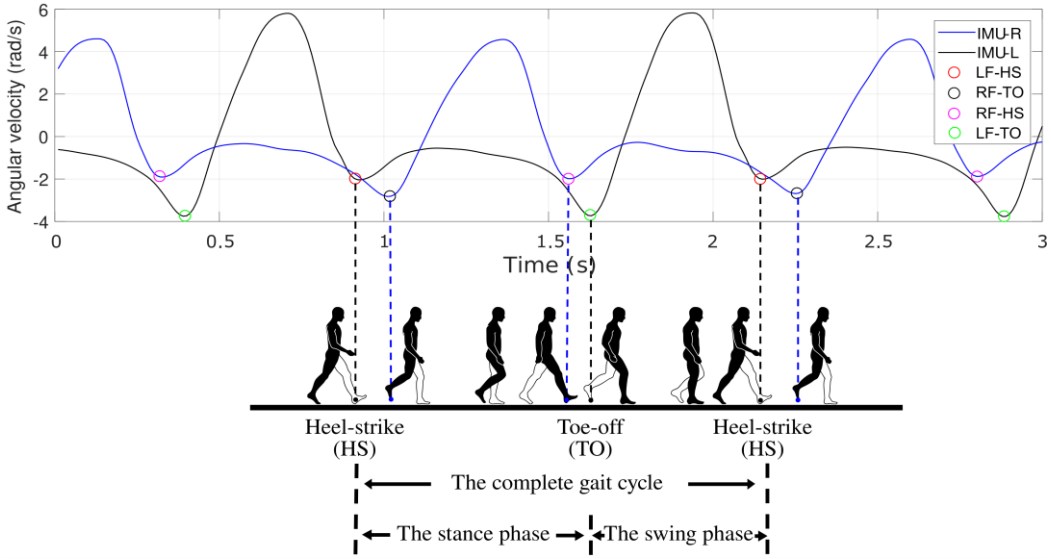

(a) Representation of the detected events using the IMU–based system.

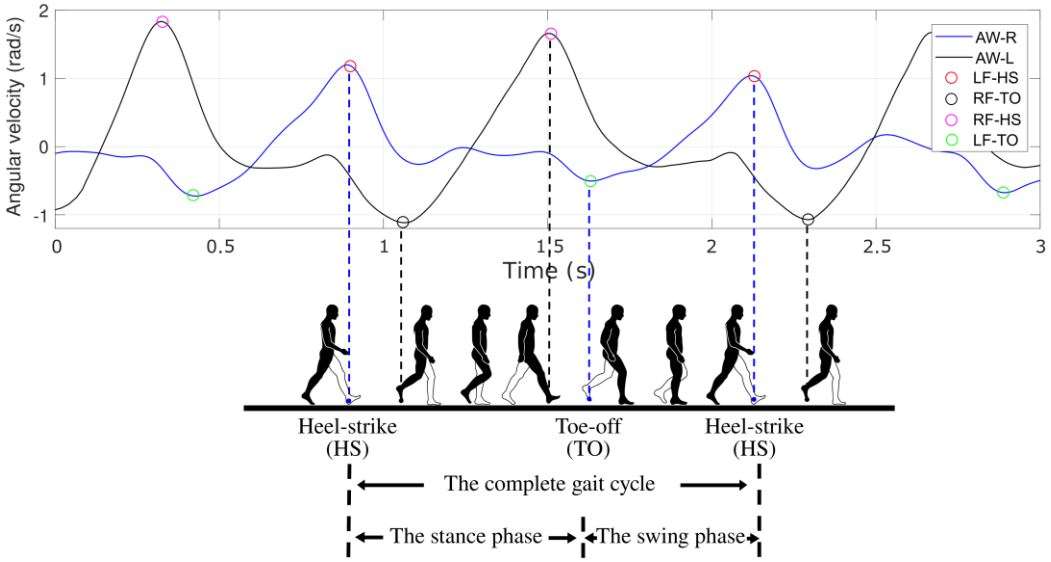

(b) Representation of the detected events using the AW–based system.

Figure 9. Representation of the detected events in the original velocity signals.

6. Method Performance

To evaluate the DWT–based method, a tolerance range of 30 ms was established in the detections concerning the reference system (G–WALK). For each event sequence, a confusion matrix was constructed, the results obtained for the detection of the gait cycle events using the IMU–based system are very similar, independent of the Wavelet Family used, and there are variations in the prediction of true positives (event class) ranging from 1–3 events per sequence. For the AW system, the results obtained were variations of 17–27 events per sequence can be observed when using one or the other family in the prediction of true positives.

The selection of the Wavelet Symlet Family could help to detect inflection points with lower amplitude and minimize the loss of human gait cycle events for the AW system. Likewise, we were able to correctly predict for the two systems all the true negatives (majority class), which correspond to the non–event class. From the confusion matrices found for each event sequence, recall, precision, and $F_1-\text{score}$ metrics were obtained, and temporal differences between the reference value and the DWT–based method were extracted. The results obtained for each method using the Wavelet Families are presented independently in Tables 2, 3, 4, and 5.

Table 2. Performance obtained from the IMU–based system using Symlets Wavelets.

Metric measures	RF–HS	LF–HS	RF–TO	LF–TO	Average
Recall (%)	94.652	94.323	94.202	94.460	94.409
Precision (%)	100	100	100	100	100
$F_1-\text{score}$ (%)	97.252	97.078	97.014	97.151	97.123
Delay (ms $\pm$ ms)	15.567 $\pm$ 4.944	15.789 $\pm$ 4.927	14.972 $\pm$ 4.963	14.765 $\pm$ 4.971	15.273 $\pm$ 4.951

Table 3. Performance obtained from the IMU–based system using Daubechies Wavelets.

Metric measures	RF–HS	LF–HS	RF–TO	LF–TO	Average
Recall (%)	94.633	94.294	94.173	94.450	94.387
Precision (%)	100	100	100	100	100
$F_1-\text{score}$ (%)	97.242	97.063	96.999	97.146	97.112
Delay (ms $\pm$ ms)	15.557 $\pm$ 4.948	15.774 $\pm$ 4.929	14.964 $\pm$ 4.961	14.760 $\pm$ 4.969	15.263 $\pm$ 4.951

For Tables 2 and 3, it can be observed that independent of the Wavelets Family used, the performance metrics for the IMU–based system are above 94 % and 100 %, for recall and precision respectively. The high percentage of precision is large because the non–event class (true negatives) is the majority class. In addition, an average $F_1-\text{score}$ metric of 97.117 % was obtained, indicating high accuracy and recall in predicting true positives. On the other hand, average event detection absolute values delays of $15.268 \pm 4.951\ ms$, i.e., 10–20 ms after the reference system, were obtained. This shows that only 5.589 % and 5.611 % errors were made in the detection using the Symlets and Daubechies Wavelet Families, respectively, out of a total of 41293 human gait cycle events immersed in the signals.

Table 4. Performance obtained from the AW–based system using Symlets Wavelets.

Metric measures	RF–HS	LF–HS	RF–TO	LF–TO	Average
Recall (%)	90.988	90.536	90.111	89.478	90.278
Precision (%)	100	100	100	100	100
$F_1-\text{score}$ (%)	95.281	95.033	94.798	94.447	94.889
Delay (ms $\pm$ ms)	16.961 $\pm$ 8.932	17.477 $\pm$ 8.801	18.315 $\pm$ 9.518	18.562 $\pm$ 9.533	17.828 $\pm$ 9.196

Table 5. Performance obtained from the AW–based system using Daubechies Wavelets.

Metric measures	RF–HS	LF–HS	RF–TO	LF–TO	Average
Recall (%)	90.758	90.277	89.945	89.253	90.058
Precision (%)	100	100	100	100	100
F_1-score (%)	95.155	94.890	94.706	94.321	94.768
Delay (ms $\pm$ ms)	17.102 $\pm$ 8.956	17.656 $\pm$ 8.870	18.418 $\pm$ 9.526	18.647 $\pm$ 9.560	17.955 $\pm$ 9.228

The AW system is presented in Tables 4 and 5. In them, it can be seen that by using one or the other Wavelet Family, more events of the gait cycle could be detected. An average performance of 90.168 % for recall and 94.828 % for F_1-score was obtained. Likewise, average absolute values delays of $17.891 \pm 9.212\ ms$, i.e., approximately 10–28 ms, were obtained. Furthermore, the errors committed were higher compared to the IMU–based system, as 9.715 % and 9.936 % errors were obtained in the detection using the Symlets and Daubechies Wavelet Families, respectively, out of a total of 41293 events. Also, the two systems have a high ability to distinguish between event and non–event classes. These results are largely due to the signal synchronization method, the detection of the MSw and HS events for the system based on IMUs and AW respectively, and the implementation of symmetric windows of 0.4 s to locate the HS and TO events.

7. Discussion

The results obtained showed significant improvements compared to previous studies, as shown in Table 6. For the two methods developed in the present study, it is emphasized that the dataset was acquired in an uncontrolled environment that may be the most appropriate for collecting and studying gait–related problems in a natural environment [59], [60], rather than in restricted and tightly controlled laboratory conditions. In addition, there were used low power consumption, low cost, and easy–to–use devices. Other authors have used different configurations for the detection of human gait events, from treadmills to pressure sensors, wearable sensors, or sensors embedded within mobile devices [6], [22], [23], [61], [62]. In [49], a system based on inertial sensors and standard motion analysis equipment based on video cameras was implemented. In [63], a method based on statistical thresholds and a zero-crossing method was used to identify two gait cycle events: HS and TO. This was from real–time measurements collected by two triaxial gyroscopes placed on the right thigh of the leg while walking on a treadmill. In [43] a useful clinical tool was developed to monitor people's walking disabilities and detect specific pathological gait patterns using an IMU in the heel. Although the results are similar to other investigations, this study is one of the first to establish a method of characterizing gait cycle events using AW signals in healthy patients.

From this table, it can be inferred that the proposed method demonstrated good performance in uncontrolled settings and healthy patients, compared to previously validated studies. In addition, it was possible to replicate the results of [49], with average absolute values delays between 10 and 20 ms, and [51], with average delays of 30 ms in the detection of HS and TO events for the IMU–based system. However, there is an important methodological difference in the first study, since it was performed in a controlled environment, which can make the gait pattern appear awkward, forced, and unnatural. Likewise, a decrease in delay times is observed, in comparison with research carried out by other authors [15], [46], [50], [64]. On the other hand, a tolerance range of 20 ms lower than those reported in [15], [22], [49] was established. Regarding performance metrics, an average for recall, precision, and F_1-score of 94.398 %, 100 %, and 97.117 %, respectively, was obtained, exceeding the results reported in [48], [65].

For the results obtained for the AW system, the following contributions are observed. First, it is one of the first pieces of research that establishes a method for detecting gait cycle events using smartwatches. Secondly, results similar to those presented in [15], [50], [64] were obtained and improved with regard to [46], with absolute values delays of approximately 10–28 ms in event detection. Finally, an average F_1-score of 94.828 % was obtained, improving and equaling the results obtained in [48], [65], respectively.

Table 6. Comparison with other studies on gait events detection using DWT. We abbreviate the references as Ref., the subject class as Sub. class, and list the IDs of each related subject class. 1: healthy subject and 2: pathological subject. The test environment is abbreviated as Test env., with the IDs of each related test environment listed, yes: for controlled and no: for uncontrolled. The tolerance ranges are abbreviated as Tol. ranges.

Ref.	Sub. class	Sensor position	Measuring system	Wavelets family	Test env.	Events detected	Metrics and Result	Delays	Tol. ranges
[64]	①	Heel and toe (toes)	Force platform	Biortogonal (bior2.6)	Yes	HS and TO	–	29 ms	–
[50]	①	Waist	IMU	Gaussian (gaus1)	No	HS and TO	–	20–30 ms	–
[48]	①	Ankle and waist (L3)	IMU	Daubechies (db2)	Yes	HS and TO	F_1- score 90 %	–	50 ms
[51]	①	Right and left ankle	IMU	Morlet (morl)	No	HS and TO	–	30 ms	60 ms
[65]	① ②	Lower back	IMU and video–cameras	Gaussian (gaus2)	Yes	HS and TO	Accuracy 88/89 % Recall 90/90 % Specificity 83/88 %	90–100 ms	–
[49]	①	Spine (L5)	IMU and video–cameras	Morlet (morl)	Yes	HS and TO	–	10 ms	50 ms
[15]	①	Spine (L5)	IMU and video–cameras	Gaussian (gaus1)	Yes	HS and TO	–	22–25 ms	50 ms
[46]	① ②	Tibialis anterior	IMU and force platform	Daubechies (db6–db5)	Yes	HS and TO	–	70–130 ms 190–330 ms	–
This study	①	Spine (L5), wrists and ankles	IMU and AW	Symlets and Daubechies (sym4 and db5)	No	HS and TO	Recall 94.398 /90.168 % Precision 100 /100 % F_1- score 97.117 /94.828 %	10–20 ms 10–28 ms	30 ms

8. Conclusions

Based on the analysis of the obtained results, the performance of the event detection method developed in this study is promising for the IMU–based system and innovative in terms of the development of the AW–based method.

The analysis of the inertial signals and the synchronization method performed in this study could be useful for the development of prototypes using inertial sensors, due to their portable characteristics, low cost, and convenience during configuration and data acquisition procedures. Likewise, the relationship found between the *z*–axis angular velocity signal obtained by the AW placed on the wrist, with the morphology of the IMU signal located at the ankles, could be useful in future research, for example, to measure the functional level of a person, the efficiency and effects of rehabilitation therapy, the detection of spatiotemporal characteristics and the frequency domain of human gait, which allow inferences about the stage of the person.

DWT–based analysis of gait cycle events, using the Symlets and Daubechies Wavelet Families provided a variety of options for decomposition and reconstruction of the angular velocity signal. This technique allowed us to decompose the signal into different frequency ranges to extract only the important information that is implicit within a defined range. From the extracted information it was possible to reconstruct a signal with the maximum and minimum peaks where the temporal events of the marching cycle of interest occurred. Among the main findings, we can highlight that: (i) decomposing the signal into 6 levels made it possible to visualize the signal dynamics and identify the relevant characteristics of the gait cycle from 6 different ranges of frequencies, (ii) the frequency range defined in the interval from 0.781 Hz to 6.250 Hz allowed to extract the relevant information of the human gait cycle and, (iii) independent of the Wavelet Family used for the IMU–based system, the reconstructed signal shows the same behavior; for the AW system, minimal variations were observed in the reconstructed signal that could improve the detection of gait cycle events when using one or the other family. In this sense, the decomposition of the angular velocity signal in different frequency ranges and the observation of the signal behavior in each of those ranges is also a relevant contribution to this work, since the selection of the decomposition levels and the frequency ranges mentioned are tedious tasks and, in some cases, are omitted or not mentioned in previous studies.

The use of automatic thresholds to characterize the events from the reconstructed DWT signals allowed the localization of the MSw and HS events for the IMUs and AW–based system, respectively, based on the summation of the mean value and the standard deviation for each signal. This selection was made taking into account that these events maintain a constant magnitude throughout the signal, unlike the HS, and TO events for the IMU–based system and TO for the AW, which could not accurately establish an automatic threshold for each event. To counteract the limitation of the method, symmetric windows of 0.4 s were established from the location of the MSw and HS events, which allowed finding the positions of the events close to the characterized event. The selection not only allowed characterizing and locating the events but also contributed to minimizing the error in the detections of HS and TO events, as these events present changes in magnitude caused by the location of the devices in different parts of the body, especially for the signals coming from AW which presented significant changes in their magnitude.

Finally, the proposed detection method based on DWT was able to detect the HS and TO events immersed in the angular velocity signal. For the IMU–based system using Wavelet Symlets, it was possible to obtain average performance metrics of 94.409 % for recall, 100 % for precision, 97.123 % for $F_1-\text{score}$, and event detection delays of $15.273 \pm 4.951\ ms$ with respect to the reference system. For Wavelet Daubechies an average performance of 94.378 % for recall, 100% for precision, 97.112 % for $F_1-\text{score}$, and detection delays of $15.263 \pm 4.951\ ms$ was achieved. It was observed that, regardless of the Wavelet Family used, the results obtained for the IMU–based system are similar, with only 9 events of difference in detection when using one or the other family. For the AW–based system, an average of 90.278 % was obtained for recall, 100 % for precision, 94.889 % for $F_1-\text{score}$, and delays of $17.828 \pm 9.196\ ms$, using Wavelet Symlets. For the Wavelet Daubechies, it was possible to obtain a recall of 90.058 %, 100 % for precision, 94.768 % for $F_1-\text{score}$, and delays of $17.955 \pm 9.228\ ms$. The result obtained showed a difference of 91 events in detection when selecting one or the other family. The selection of Wavelet Symlets could help to improve the detection of peaks with lower magnitudes in the signal.

Other contributions of this study are: Other contributions to this study are the synchronization method, the labels extracted by the SMARTanalyzer® software, and the morphology of the angular velocity signal, which allowed determining the condition of advance or delay, concerning the reference signal. With this, the synchronization error was minimized since no protocol was established for the initialization of the acquisition of information of the instruments during the test. A relationship was found between the angular velocity signal in the *z*–axis obtained by the AW placed on the wrist, with the morphology of the IMU signal, located in the ankles. This

allowed the identification of the main characteristics of the gait signal, such as stance and swing phases and the inflection points associated with the HS and TO events.

9. Limitations

Limitations of this study include that the performance obtained for the AW system could be associated with factors such as stiffness, asymmetry in the upper limbs, or problems in the measuring devices. In addition, data acquisition was performed in a natural environment, where the person was moving overground over a 30–meter straight hallway at three different speeds (slow, normal, and fast) with no restrictions for 6 minutes. The tests should be performed in a controlled environment to validate the aforementioned hypothesis. On the other hand, the test was only performed on middle–aged people with no history of neuromuscular disorders or gait abnormality, so in order to achieve a generalization of the method, tests should be performed on people of different age groups.

Declaration of competing interest

The authors declare that they have no any known financial or non-financial competing interests in any material discussed in this paper.

Funding information

No funding was received from any financial organization to conduct this research.

References

[1] A. H. Snijders, B. P. van de Warrenburg, N. Giladi, and B. R. Bloem, "Neurological gait disorders in elderly people: clinical approach and classification," *Lancet Neurol.*, vol. 6, no. 1, pp. 63–74, 2007, doi: 10.1016/S1474-4422(06)70678-0.

[2] J. C. Arellano-González, H. I. Medellín-Castillo, and J. J. Cervantes-Sánchez, "Identification and analysis of biomechanical parameters used for the evaluation of normal and pathological human gait," *Memorias del XXV Congr. Int. Anu. la SOMIM*, pp. 1–9, 2019.

[3] S. R. Subirana and M. àngel M. Adell, "Assessment of gait in the elderly," *FMC Form. Medica Contin. en Aten. Primaria*, vol. 27, no. 1, pp. 4–10, 2020, doi: 10.1016/j.fmc.2019.05.013.

[4] L. Z. Rubenstein, A. S. Robbins, B. L. Schulman, J. Rosado, D. Osterweil, and K. R. Josephson, "Falls and instability in the elderly," *Am. Geriatr. Soc.*, vol. 36, no. 1, pp. 266–279, 1988, doi: 10.1111/j.1532-5415.1988.tb01811.x.

[5] J. M. Hausdorff, D. A. Rios, and H. K. Edelberg, "Gait variability and fall risk in community-living older adults: A 1-year prospective study," *Arch. Phys. Med. Rehabil.*, vol. 82, no. 8, pp. 1050–1056, 2001, doi: 10.1053/apmr.2001.24893.

[6] A. Mannini, D. Trojaniello, A. Cereatti, and A. M. Sabatini, "A machine learning framework for gait classification using inertial sensors: Application to elderly, post-stroke and huntington's disease patients," *Sensors (Switzerland)*, vol. 16, no. 1, 2016, doi: 10.3390/s16010134.

[7] C. Cui *et al.*, "Simultaneous Recognition and Assessment of Post-Stroke Hemiparetic Gait by Fusing Kinematic, Kinetic, and Electrophysiological Data," *IEEE Trans. Neural Syst. Rehabil. Eng.*, vol. 26, no. 4, pp. 856–864, 2018, doi: 10.1109/TNSRE.2018.2811415.

[8] D. Rincón *et al.*, "Wristbands containing accelerometers for objective arm swing analysis in patients with parkinson's disease," *Sensors (Switzerland)*, vol. 20, no. 15, pp. 1–14, 2020, doi: 10.3390/s20154339.

[9] Z. Cao *et al.*, "Identification of EEG Dynamics During Freezing of Gait and Voluntary Stopping in Patients With Parkinson's Disease," *IEEE Trans. Neural Syst. Rehabil. Eng.*, vol. 29, pp. 1774–1783, 2021, doi: 10.1109/TNSRE.2021.3107106.

[10] T. S. de Paiva, R. S. Gonçalves, G. Carbone, and M. Ceccarelli, "Chapter 4 - Gait devices for stroke rehabilitation: State-of-the-art, challenges, and open issues," in *Medical and Healthcare Robotics*, O. Boubaker, Ed., in Medical Robots and Devices: New Developments and Advances. , Academic Press, 2023, pp. 87–122. doi: https://doi.org/10.1016/B978-0-443-18460-4.00003-2.

[11] G. V Prateek, P. Mazzoni, G. M. Earhart, and A. Nehorai, "Gait Cycle Validation and Segmentation

Using Inertial Sensors," *IEEE Trans. Biomed. Eng.*, vol. 67, no. 8, pp. 2132–2144, 2020, doi: 10.1109/TBME.2019.2955423.

[12] J. C. Pérez-Ibarra, A. A. G. Siqueira, and H. I. Krebs, "Identification of Gait Events in Healthy Subjects and With Parkinson's Disease Using Inertial Sensors: An Adaptive Unsupervised Learning Approach," *IEEE Trans. Neural Syst. Rehabil. Eng.*, vol. 28, no. 12, pp. 2933–2943, 2020, doi: 10.1109/TNSRE.2020.3039999.

[13] S. K. Bansal, B. Basumatary, R. Bansal, and A. K. Sahani, "Techniques for the detection and management of freezing of gait in Parkinson's disease – A systematic review and future perspectives," *MethodsX*, vol. 10, p. 102106, 2023, doi: https://doi.org/10.1016/j.mex.2023.102106.

[14] L. Sigcha *et al.*, "Deep learning and wearable sensors for the diagnosis and monitoring of Parkinson's disease: A systematic review," *Expert Syst. Appl.*, vol. 229, p. 120541, 2023, doi: https://doi.org/10.1016/j.eswa.2023.120541.

[15] C. Caramia, C. De Marchis, and M. Schmid, "Optimizing the scale of a wavelet-based method for the detection of gait events from a waist-mounted accelerometer under different walking speeds," *Sensors (Switzerland)*, vol. 19, no. 8, 2019, doi: 10.3390/s19081869.

[16] N. Richer, R. J. Downey, W. D. Hairston, D. P. Ferris, and A. D. Nordin, "Motion and Muscle Artifact Removal Validation Using an Electrical Head Phantom, Robotic Motion Platform, and Dual Layer Mobile EEG," *IEEE Trans. Neural Syst. Rehabil. Eng.*, vol. 28, no. 8, pp. 1825–1835, 2020, doi: 10.1109/TNSRE.2020.3000971.

[17] C. Caramia, I. Bernabucci, C. D'Anna, C. De Marchis, and M. Schmid, "Gait parameters are differently affected by concurrent smartphone-based activities with scaled levels of cognitive effort," *PLoS One*, vol. 12, no. 10, pp. 1–2, 2017, doi: 10.1371/journal.pone.0185825.

[18] D. R. Cyril Voisard Nicolas de l'Escalopier and L. Oudre, "Automatic gait events detection with inertial measurement units: healthy subjects and moderate to severe impaired patients," *J. Neuroeng. Rehabil.*, vol. 21, no. 104, 2024, doi: 10.1186/s12984-024-01405-x.

[19] J. M. Bond and M. Morn's, "Goal-directed secondary motor tasks: Their effects on gait in subjects with Parkinson disease," *Arch. Phys. Med. Rehabil.*, vol. 81, no. 1, pp. 110–116, 2000, doi: 10.1053/apmr.2000.0810110.

[20] F. Marin, K. Lepetit, L. Fradet, C. Hansen, and K. Ben Mansour, "Using accelerations of single inertial measurement units to determine the intensity level of light-moderate-vigorous physical activities: Technical and mathematical considerations," *J. Biomech.*, vol. 107, p. 109834, 2020, doi: https://doi.org/10.1016/j.jbiomech.2020.109834.

[21] W. J. Jaimes, J. F. Mantilla, S. A. Salinas, and H. J. Navarro, "Modeling and Simulation of a Lower Limb Exoskeleton with Computed Torque Control for Gait Rehabilitation," *2021 Glob. Med. Eng. Phys. Exch. Am. Heal. Care Exch.*, pp. 1–6, 2021, doi: 10.1109/GMEPE/PAHCE50215.2021.9434854.

[22] D. Trojaniello *et al.*, "Estimation of step-by-step spazio-temporal parameters of normal and impaired gait using shank-mounted magneto-inertial sensors," *J. Neuroeng Rehabil*, vol. 11, no. 152, pp. 1–12, 2014.

[23] N. C. Bejarano, E. Ambrosini, A. Pedrocchi, G. Ferrigno, M. Monticone, and S. Ferrante, "A novel adaptive, real-time algorithm to detect gait events from wearable sensors," *IEEE Trans. Neural Syst. Rehabil. Eng.*, vol. 23, no. 3, pp. 413–422, 2015, doi: 10.1109/TNSRE.2014.2337914.

[24] S. R. Donahue and M. E. Hahn, "Feature Identification With a Heuristic Algorithm and an Unsupervised Machine Learning Algorithm for Prior Knowledge of Gait Events," *IEEE Trans. Neural Syst. Rehabil. Eng.*, vol. 30, pp. 108–114, 2022, doi: 10.1109/TNSRE.2021.3131953.

[25] W. Maetzler, J. Klucken, and M. Horne, "A clinical view on the development of technology-based tools in managing Parkinson's disease," *Mov. Disord.*, vol. 31, no. 9, pp. 1263–1271, 2016, doi: 10.1002/mds.26673.

[26] U. Q. Shaikh, M. Shahzaib, S. Shakil, F. A. Bhatti, and M. Aamir Saeed, "Robust and adaptive terrain classification and gait event detection system," *Heliyon*, vol. 9, no. 11, p. e21720, 2023, doi: https://doi.org/10.1016/j.heliyon.2023.e21720.

[27] G. Prigent *et al.*, "A robust walking detection algorithm using a single foot-worn inertial sensor: validation in real-life settings," *Med. Biol. Eng. Comput.*, vol. 61, pp. 2341–2352, 2023, doi:

10.1007/s11517-023-02826-x.

[28] L. J. Vargas Escobar, "System for measuring time parameters of human gait," Universidad Pontificia Bolivariana, 2017.

[29] H. J. Navarro *et al.*, "Gait events detection using inertial sensors, Apple Watch, and the G-WALK reference system," *2021 Glob. Med. Eng. Phys. Exch. Am. Heal. Care Exch.*, pp. 1–6, 2021, doi: 10.1109/GMEPE/PAHCE50215.2021.9434858.

[30] R. Schwesig, S. Leuchte, D. Fischer, R. Ullmann, and A. Kluttig, "Inertial sensor based reference gait data for healthy subjects," *Gait Posture*, vol. 33, no. 4, pp. 673–678, 2011, doi: 10.1016/j.gaitpost.2011.02.023.

[31] Q. Riaz, A. Vögele, B. Krüger, and A. Weber, "One small step for a man: Estimation of gender, age and height from recordings of one step by a single inertial sensor," *Sensors (Switzerland)*, vol. 15, no. 12, pp. 31999–32019, 2015, doi: 10.3390/s151229907.

[32] M. Lozano-García *et al.*, "Estimation of Gait Parameters in Huntington's Disease Using Wearable Sensors in the Clinic and Free-living Conditions," *IEEE Trans. Neural Syst. Rehabil. Eng.*, vol. 32, pp. 2239–2249, 2024, doi: 10.1109/TNSRE.2024.3407887.

[33] R. W. Bohannon, "Comfortable and maximum walking speed of adults aged 20-79 years: Reference values and determinants," *Age Ageing*, vol. 26, no. 1, pp. 15–19, 1997, doi: 10.1093/ageing/26.1.15.

[34] S. Fritz and M. Lusardi, "White paper: walking speed: The sixth vital sign," *J. Geriatr. Phys. Ther.*, vol. 32, no. 2, pp. 2–5, 2009, doi: 10.1519/00139143-200932020-00002.

[35] P. Medina González, "Evaluation of comfortable and maximum gait kinematics parameters in functionally independent elderly Chileans," *Fisioterapia*, vol. 38, no. 6, pp. 286–294, 2016, doi: 10.1016/j.ft.2015.11.002.

[36] J. Daza Lesmes, *Clinical-functional evaluation of human body movement*. Bogotá: Médica Panamericana, 2007.

[37] T. Stöckel, R. Jacksteit, M. Behrens, R. Skripitz, R. Bader, and A. Mau-Moeller, "The mental representation of the human gait in young and older adults," *Front. Psychol.*, vol. 6, 2015, doi: 10.3389/fpsyg.2015.00943.

[38] J. P. Kuhtz-Buschbeck and B. Jing, "Activity of upper limb muscles during human walking," *J. Electromyogr. Kinesiol.*, vol. 22, no. 2, pp. 199–206, 2012, doi: 10.1016/j.jelekin.2011.08.014.

[39] J. P. Kuhtz-Buschbeck, K. Brockmann, R. Gilster, A. Koch, and H. Stolze, "Asymmetry of arm-swing not related to handedness," *Gait Posture*, vol. 27, no. 3, pp. 447–454, 2008, doi: 10.1016/j.gaitpost.2007.05.011.

[40] I. P. I. Pappas, M. R. Popovic, T. Keller, V. Dietz, and M. Morari, "A reliable gait phase detection system," *IEEE Trans. Neural Syst. Rehabil. Eng.*, vol. 9, no. 2, pp. 113–125, 2001, doi: 10.1109/7333.928571.

[41] K. Aminian, B. Najafi, C. Büla, P. F. Leyvraz, and P. Robert, "Spatio-temporal parameters of gait measured by an ambulatory system using miniature gyroscopes," *J. Biomech.*, vol. 35, no. 5, pp. 689–699, 2002, doi: 10.1016/S0021-9290(02)00008-8.

[42] H. Lau and K. Tong, "The reliability of using accelerometer and gyroscope for gait event identification on persons with dropped foot," *Gait Posture*, vol. 27, no. 2, pp. 248–257, 2008, doi: 10.1016/j.gaitpost.2007.03.018.

[43] R. Soangra, T. E. Lockhart, and N. Van De Berge, "An approach for identifying gait events using wavelet denoising technique and single wireless IMU," *Proc. Hum. Factors Ergon. Soc.*, pp. 1990–1994, 2011, doi: 10.1177/1071181311551415.

[44] M. A. D. Brodie *et al.*, "Wearable pendant device monitoring using new wavelet-based methods shows daily life and laboratory gaits are different," *Med. Biol. Eng. Comput.*, vol. 54, no. 4, pp. 663–674, 2016, doi: 10.1007/s11517-015-1357-9.

[45] Y. J. Castaño-Pino, A. Navarro, B. Muñoz, and J. L. Orozco, *Using Wavelets for Gait and Arm Swing Analysis*. IntechOpen, 2019. doi: 10.5772/intechopen.84962.

[46] N. Ji *et al.*, "Appropriate mother wavelets for continuous gait event detection based on time-frequency analysis for hemiplegic and healthy individuals," *Sensors (Switzerland)*, vol. 19, no. 16, pp. 1–18, 2019,

doi: 10.3390/s19163462.

[47] J. Chakraborty and A. Nandy, "Discrete wavelet transform based data representation in deep neural network for gait abnormality detection," *Biomed. Signal Process. Control*, vol. 62, p. 102076, 2020, doi: 10.1016/j.bspc.2020.102076.

[48] M. S. H. Aung *et al.*, "Automated detection of instantaneous gait events using time frequency analysis and manifold embedding," *IEEE Trans. Neural Syst. Rehabil. Eng.*, vol. 21, no. 6, pp. 908–916, 2013, doi: 10.1109/TNSRE.2013.2239313.

[49] T. Sugiarto, Y. J. Lin, C. C. Chang, and W. C. Hsu, "Gait analysis based on an inertial measurement unit sensor: Validation of spatiotemporal parameters calculation in healthy young and older adults," *SII 2017 - 2017 IEEE/SICE Int. Symp. Syst. Integr.*, vol. 2018-Janua, pp. 517–522, 2018, doi: 10.1109/SII.2017.8279273.

[50] J. McCamley, M. Donati, E. Grimpampi, and C. Mazzà, "An enhanced estimate of initial contact and final contact instants of time using lower trunk inertial sensor data," *Gait Posture*, vol. 36, no. 2, pp. 316–318, 2012, doi: 10.1016/j.gaitpost.2012.02.019.

[51] S. Khandelwal and N. Wickström, "Gait Event Detection in Real-World Environment for Long-Term Applications: Incorporating Domain Knowledge Into Time-Frequency Analysis," *IEEE Trans. Neural Syst. Rehabil. Eng.*, vol. 24, no. 12, pp. 1363–1372, 2016, doi: 10.1109/TNSRE.2016.2536278.

[52] M. S. Chavan, N. Mastorakis, M. N. Chavan, and M. S. Gaikwad, "Implementation of SYMLET wavelets to removal of Gaussian additive noise from speech signal," *10th WSEAS Int. Conf. EHAC'11 ISPRA'11, 3rd WSEAS Int. Conf. Nanotechnology, Nanotechnology'11, 6th WSEAS Int. Conf. ICOAA'11, 2nd WSEAS Int.Conf. IPLAFUN'11*, no. September 2016, pp. 37–41, 2011.

[53] F. Riveros Sanabria, "Wavelet analysis of electrocardiographic alterations in chronic chagasic patients," Universidad EAFIT, Medellín, 2012.

[54] D. A. Bruening, R. E. Frimenko, C. D. Goodyear, D. R. Bowden, and A. M. Fullenkamp, "Sex differences in whole body gait kinematics at preferred speeds," *Gait Posture*, vol. 41, no. 2, pp. 540–545, 2015, doi: 10.1016/j.gaitpost.2014.12.011.

[55] M. D. Lewek, R. Poole, J. Johnson, O. Halawa, and X. Huang, "Arm swing magnitude and asymmetry during gait in the early stages of Parkinson's disease," *Gait Posture*, vol. 31, no. 2, pp. 256–260, 2010, doi: 10.1016/j.gaitpost.2009.10.013.

[56] T. L. Riley, W. F. Ray, and E. W. Massey, "Gait mechanisms: asymmetry of arm motion in normal subjects.," *Mil Med.*, vol. 142, no. 6, pp. 467–468, 1977, [Online]. Available: https://pubmed.ncbi.nlm.nih.gov/407495/

[57] J. L. Stephenson, S. J. De Serres, and A. Lamontagne, "The effect of arm movements on the lower limb during gait after a stroke," *Gait Posture*, vol. 31, no. 1, pp. 109–115, 2010, doi: 10.1016/j.gaitpost.2009.09.008.

[58] M. Goudriaan, I. Jonkers, J. H. van Dieen, and S. M. Bruijn, "Arm swing in human walking: What is their drive?," *Gait Posture*, vol. 40, no. 2, pp. 321–326, 2014, doi: 10.1016/j.gaitpost.2014.04.204.

[59] J. Rueterbories, E. G. Spaich, and O. K. Andersen, "Gait event detection for use in FES rehabilitation by radial and tangential foot accelerations," *Med. Eng. Phys.*, vol. 36, no. 4, pp. 502–508, 2014, doi: 10.1016/j.medengphy.2013.10.004.

[60] S. Qiu, Z. Wang, H. Zhao, K. Qin, Z. Li, and H. Hu, "Inertial/magnetic sensors based pedestrian dead reckoning by means of multi-sensor fusion," *Inf. Fusion*, vol. 39, pp. 108–119, 2018, doi: 10.1016/j.inffus.2017.04.006.

[61] Y. Gao *et al.*, "A Novel Gait Detection Algorithm Based on Wireless Inertial Sensors," *Badnjevic A*, vol. 62, pp. 300–304, 2017, doi: 10.1007/978-981-10-4166-2_45.

[62] R. Caldas, M. Mundt, W. Potthast, F. Buarque de Lima Neto, and B. Markert, "A systematic review of gait analysis methods based on inertial sensors and adaptive algorithms," *Gait Posture*, vol. 57, no. June, pp. 204–210, 2017, doi: 10.1016/j.gaitpost.2017.06.019.

[63] D. Gouwanda and A. A. Gopalai, "A robustreal-time gaiteventdetection using wirelessgyroscope and itsapplication on normal and alteredgaits," *Med. Eng. Phys.*, vol. 37, no. 2, pp. 219–225, 2015, doi: 10.1016/j.medengphy.2014.12.004.

[64] P. M. Forsman, E. M. Toppila, and E. O. Hæggström, "Wavelet analysis to detect gait events," *Proc.*

31st Annu. Int. Conf. IEEE Eng. Med. Biol. Soc. Eng. Futur. Biomed. EMBC 2009, pp. 424–427, 2009, doi: 10.1109/IEMBS.2009.5333137.

[65] M. H. Pham *et al.*, "Validation of a step detection algorithm during straight walking and turning in Patients with Parkinson's disease and older adults using an inertial measurement unit at the lower back," *Front. Neurol.*, vol. 8, no. SEP, pp. 1–9, 2017, doi: 10.3389/fneur.2017.00457.